Modelling Simul. Mater. Sci. Eng. **19** (2011) 065006 (14pp) doi:10.1088/0965-0393/19/6/065006

Equilibrium shape of dislocation shear loops in anisotropic α-Fe

S Aubry[1], S P Fitzgerald[2], S L Dudarev[2] and W Cai[1]

[1] Department of Mechanical Engineering, Stanford University, CA, USA
[2] EURATOM/CCFE Fusion Association, Culham Centre for Fusion Energy, Abingdon OX14 3DB, UK

Received 7 December 2010, in final form 22 June 2011
Published 2 August 2011
Online at stacks.iop.org/MSMSE/19/065006

Abstract
We present dislocation dynamics (DD) simulations of shear loops in a highly anisotropic linear elastic crystal. The equilibrium shapes of the loops are determined for the four principal slip systems of the body-centered-cubic lattice, using empirical elastic constants for α-Fe, for a range of temperatures over which its elastic anisotropy varies considerably. The results are compared with those obtained from the isotropic elasticity approximation, and from an analytical line tension model. Sharp corners, which have been observed in the electron microscope and arise due to the thermodynamic instability of certain dislocation orientations, are reproduced by DD simulations in qualitative agreement with existing analytical calculations. Some differences are observed between the DD and the line tension model predictions.

1. Introduction

As the α–γ phase transition in iron at 912 °C is approached, the tetragonal shear modulus $C' = (C_{11} - C_{12})/2$ falls sharply towards zero while the trigonal shear modulus C_{44} remains relatively close to its low-temperature value (figure 1) [1]. This is due to the displacive nature of the transformation: tetragonal displacements are conducive to the change in crystal structure, and experience less resistance from the lattice as the transition temperature is approached. The large difference between the two shear moduli (which reaches a factor of more than 7) means that the isotropic approximation to elasticity theory does not apply. The mechanical properties at high elastic anisotropy can differ substantially from those of the isotropic limit, a fact of special significance for the development of high-temperature ferritic–martensitic steels for advanced fission and fusion reactors. In particular, steels which exhibit an α–γ phase transition suffer a pronounced loss of strength as the transition temperature is approached [2], a phenomenon which has been attributed to anisotropic dislocation behavior [3, 4].

The equilibrium shapes adopted by crystal dislocations strongly depend on the elastic properties of the crystal lattice. In particular, sharp corners betray thermodynamic instabilities

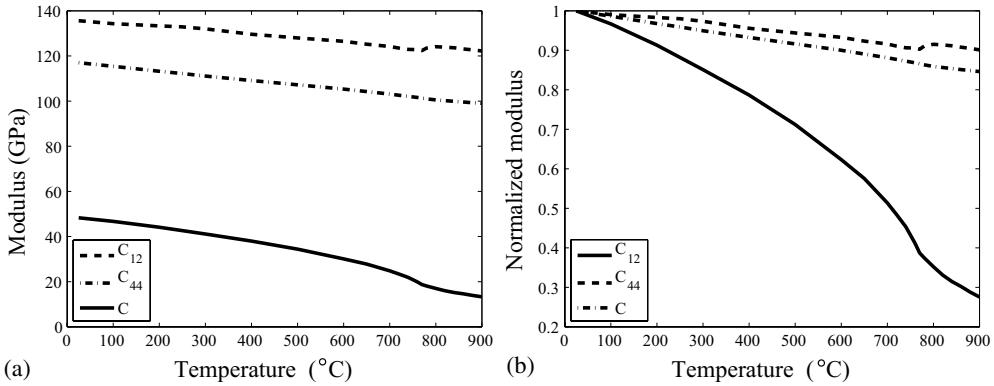

Figure 1. Elastic moduli of α-Fe from 25 to 900 °C [1]. Elastic isotropy would require $C_{44} = C'$. (*a*) Absolute values. Note that at 25 °C Fe is already significantly anisotropic ($C_{44}/C' \sim 2.4$) and as the transition at 912 °C is approached, $C_{44}/C' \sim 7.4$. (*b*) Moduli normalized to 25 °C values. The convex fall of C' up to the Curie point (770 °C) is consistent with the nature of the phase transition. Above this point the curve begins to level off but continues falling until the final measurement at 900 °C [5].

of certain dislocation orientations in highly anisotropic crystals, such as α-Fe at elevated temperatures. Furthermore, these structures should be visible in the electron microscope, and if they are sufficiently large, their shapes are expected to be scale-free, and should apply to dislocation segments and loops of any size.

The phenomena of sharp corners and dislocation instability have investigated analytically [4, 6, 7] and in the microscope [6, 8–12], with qualitatively good agreement between theory and observation. Most of the theoretical work is based on a local line tension approximation, where interactions between different parts of the dislocation are neglected. In this paper, we report dislocation dynamics (DD) simulations of loops in highly anisotropic α-Fe, where interactions are taken fully into account.

The anisotropic continuum theory of dislocations has been developed over several decades (for a review see for example [13]). Several attempts have been made to develop DD simulation programs [14, 15] based on anisotropic elasticity, but the computational cost is much higher than for DD simulations using only isotropic elasticity. In [16–18], we explain how anisotropic elasticity was added to `ParaDiS` and how it compares with alternative approaches. The detailed study of [14] considered various fundamental dislocation processes, including Frank–Read sources and junction formation, and concluded that elastic anisotropy principally impacted dynamic processes, whereas static equilibrium phenomena were largely insensitive to it. In this study, we focus on the equilibrium shapes of shear loops, and show that these also are significantly affected by the anisotropy, once we consider a sufficiently anisotropic crystal, such as the high-temperature α-Fe.

As well as testing the validity or otherwise of the line tension approximation, the DD method provides a more accurate and detailed model for the shear loops, and its predictions are suitable for quantitative comparison with electron microscope observations. This provides a stringent benchmark for the simulation, testing both the implementation itself and the validity of the underlying models. Furthermore, capturing the correct equilibrium shapes of dislocations is important for studies of interacting ensembles of dislocations, as it identifies which configurations are energetically favored, and hence are realized most often in a deformed crystal. This will impact on dislocation reactions, and hence must be taken into account in any attempt to model yield and work hardening in anisotropic crystals.

Our simulations confirm that sharp corners indeed arise in Fe when the temperature, and hence anisotropy, is high enough and that surprisingly, they also arise in an isotropic approximation provided the isotropic moduli are computed using Scattergood and Bacon's slip system-dependent prescription ([19], see section 4). We find that the shapes predicted by the line tension approximation are close to those found using the fully interacting DD simulations.

In the next two sections we briefly summarize the analytical approach from [4, 6, 20], the implementation of anisotropic elasticity in our DD simulation program and the relaxation algorithm we use to determine the equilibrium shapes of the loops. Using empirical elastic moduli for α-Fe, we compute the shapes for loops in the four principal orientations of the body-centered-cubic (bcc) lattice, for a range of temperatures over which the anisotropy of α-Fe varies considerably. In section 4 we compute the shapes predicted by several isotropic averages of the true moduli. In section 5 we discuss the effects of the core energy, and compare the resulting shapes with those obtained using the analytical line tension approximation. The appendix contains some technical details of the algorithms.

2. Analytical variational method based on the line tension model

A variational approach to determine the equilibrium shapes of shear loops originally developed in [20] was extended in [4] to include the sharp-cornered configurations encountered in crystals of high anisotropy. The general idea is to balance the work done by an applied stress $\boldsymbol{\sigma}$ with the energy change as a planar dislocation loop L undergoes an infinitesimal displacement. We parametrize the curve as $\boldsymbol{r}(\lambda)$, and denote the infinitesimal displacement $\delta\boldsymbol{r}(\lambda)$, where λ is any suitable monotonically increasing parameter. Adopting a local line tension model for the energy of the dislocation leads to [4]

$$0 = \oint_L \frac{\mathrm{d}}{\mathrm{d}\lambda}\left[\epsilon_{ijk}\,\sigma_{jl}\,b_l\,r_k + \frac{\partial}{\partial \dot{r}_i}\left(E\sqrt{\dot{r}_p\dot{r}_p}\right)\right]\delta r_i\,\mathrm{d}\lambda, \tag{1}$$

where $\boldsymbol{b}$ is the loop's Burgers vector and E is the energy per unit length [13], which depends only on the elastic moduli and the local line direction. The first term originates from the Peach–Koehler force due to the applied stress, and the second from the variation in the self-energy of the loop. Overdots denote derivatives taken with respect to λ, so $\dot{\boldsymbol{r}}$ is a local tangent to the line. The derivatives with respect to $\dot{\boldsymbol{r}}$ thus correspond to the *angular* dependence of the line energy. This approximation neglects interactions between different parts of the loop, and hence is a significant idealization. Yet it yields a tractable equation for the loop's shape, which can be written in terms of intrinsic coordinates (s, ψ) in the glide plane as

$$\rho \equiv \frac{\mathrm{d}s}{\mathrm{d}\psi} = \frac{1}{|\boldsymbol{\sigma}\cdot b|}\left(E + \frac{\mathrm{d}^2E}{\mathrm{d}\psi^2}\right) \equiv \frac{1}{|\boldsymbol{\sigma}\cdot b|}\Gamma(\psi), \tag{2}$$

where s is the distance along the curve and ρ is the local radius of curvature. ψ is the angle the curve makes with any fixed reference datum in the plane; we choose the datum to be the direction of the Burgers vector $\boldsymbol{b}$.

When the line tension $\Gamma(\psi)$ is positive for all ψ, as is the case for isotropic crystals[3] and those of modest anisotropy, equation (2) defines a convex planar curve. However, when the crystal is highly anisotropic, as is the case for α-Fe at high temperatures, the line tension can become negative for some orientations, leading to thermodynamically unstable directions. The dislocation can avoid these directions by introducing sharp corners.

[3] This holds for true isotropic crystals, i.e. when Poisson's ratio ν satisfies $-1 < \nu < 0.5$. When Scattergood and Bacon average moduli are used, the effective ν is no longer limited to this range, and $\Gamma(\psi)$ can become negative for certain orientations (see section 4) and equation (4).

The explicit expression for $\Gamma(\psi)$ in anisotropic elasticity is considerably more complicated than in isotropic elasticity, and only semi-analytical. It is given by the equation between equations (4.1.45) and (4.1.46) [13, p 151].

3. Simulation methodology

Our code is an extension of the DD simulation package `ParaDiS` [21] to account for anisotropic elasticity [16]. The dislocation structure is discretized, represented by a network of nodes connected by straight segments. The network evolves under the influences of the forces on its nodes, which are determined from the elastic forces acting on each segment. The origin of these forces is threefold:

(1) The force due to the external applied stress $\boldsymbol{\sigma}_{\text{ext}}$. This is given by the Peach–Koehler formula for the force per unit length on a dislocation with Burgers vector $\boldsymbol{b}$ and line direction $\boldsymbol{\xi}$: $\boldsymbol{F} = (\boldsymbol{\sigma}_{\text{ext}} \cdot \boldsymbol{b}) \wedge \boldsymbol{\xi}$.
(2) The elastic force due to the stress fields of the rest of the dislocation network. The Peach–Koehler formula still applies and the nodal forces correspond to a weighted integral of the Peach–Koehler forces.
(3) The *self-force* acting on a segment. This is caused by the Peach–Koehler force from the segment's own stress field. This self-force is perpendicular to the segment and tends to rotate the segment away from high-energy orientations. When an orientation-independent core energy is added, as is done in this study, the self-force acquires a longitudinal component, which tends to shorten the segment.

The force on a given node is calculated by combining contributions from (1), (2) and (3) over each segment connected to the node. Finally, the network is evolved according to a mobility law relating nodal force to velocity. For the simulations we report here, the mobility law is essentially a relaxation, see the appendix.

In isotropic elasticity, the stress field generated at a point $\boldsymbol{x}$ by a straight dislocation segment from $\boldsymbol{x}_A$ to $\boldsymbol{x}_B$ can be given by explicit analytical expressions. However in a general anisotropic medium, no such formula exists. The stress field generated by any dislocation configuration can be calculated via Mura's expression [22] for the strain, using the second-rank Green's function $\boldsymbol{G}$. Several methods exist to calculate $\boldsymbol{G}$, and involve either solving a sextic polynomial or performing an integral around the unit disk [13]. We use the integral method, as it is numerically robust for all dislocation orientations, whereas the sextic method requires extra care for certain high-symmetry configurations and the isotropic limit. Either method clearly introduces a significant computational cost compared with the isotropic case, which requires only the evaluation of an explicit analytical formula. When using the integral method, we take 31 uniformly distributed integration points along the unit circle. This ensures that the maximum relative error of $\mathrm{d}^2E/\mathrm{d}\psi^2$ is less than 10^{-4}.

The self-force acting on a segment can be calculated either by integrating the self-stress field (with proper cut-off) [16, 17], or by taking spatial derivative of the segment self-energy [18]. The two methods are equivalent, provided that their corresponding approaches are applied to segment–segment interactions, i.e. the interaction forces between two segments are also calculated by integrating the stress field of one segment over the other segment, or by taking spatial derivative of the segment–segment interaction energy. In this work, we use the method of integrating the self-stress field to evaluate the self-force. It is more efficient and numerically stable because it does not involve numerical derivatives.

In order to determine the equilibrium shapes of shear loops in the four slip systems in a bcc crystal, shown in table 1, we start by defining a circular loop in the appropriate slip plane,

and allow it to relax until the force on each node is zero while keeping the area of the loop constant. The energy of the loop is subsequently determined by numerical integration of the nodal forces as the loop is continuously shrunk to zero radius (see appendix).

4. Isotropic averages

Various prescriptions for calculating effective isotropic moduli for anisotropic crystals have been proposed, e.g. Voigt and Reuss average elastic moduli, which were developed to model the aggregate behavior of polycrystals. Voigt's procedure [23] assumes the strain is uniform everywhere (and results in inter-grain forces being out of equilibrium), whereas Reuss' procedure [24] assumes the stress is uniform (leading to deformed grains which do not fit together). The Voigt average μ_V is similar to the arithmetic mean of the two shear moduli, C_{44} and C', while the Reuss average μ_R is closer to the geometric mean, so it better captures the severe softening of C'. In general, the Voigt average will overestimate characteristic stresses, whereas the Reuss average will underestimate them, when compared with the values calculated using the full anisotropic theory. While useful for treating the elastic behavior of polycrystals, globally defined pair of isotropic constants cannot capture the elastic behavior of dislocations in an elastically anisotropic single crystal grain in which failure usually initiates. Scattergood and Bacon's method [19] was specifically developed with dislocations in mind, and the effective shear modulus and Poisson ratio are defined as follows:

$$\mu_S = \frac{4\pi}{|\boldsymbol{b}|^2} E_{\text{screw}} \qquad \nu_S = 1 - \frac{E_{\text{screw}}}{E_{\text{edge}}}, \tag{3}$$

where E_{screw} and E_{edge} are the pre-logarithmic part of the energy of a straight screw and a straight edge dislocation respectively in the given slip system.

Since the isotropic moduli as defined by equation (3) vary for different slip systems, they cannot truly be interpreted as effective isotropic moduli. The various average values are shown in figure 2. We note that for both [1 0 0] systems, the lattice is auxetic, i.e. it has a negative effective Poisson ratio [25]. The Scattergood and Bacon's shear modulus for a given Burgers vector is independent of the glide plane, since it depends only on the energy of a screw dislocation for that Burgers vector.

An isotropic crystal's stability depends on the Poisson ratio ν lying between -1 and 0.5. However, effective values of ν as defined above can fall outside this range without implying crystal instability. When this happens, the isotropic expression for the line tension

$$\Gamma(\psi) = \frac{\mu|\boldsymbol{b}|^2}{4\pi}\left(1 + \frac{\nu}{1-\nu}\left(3\cos^2\psi - 1\right)\right) \tag{4}$$

can become negative for some ψ values (ψ is the angle between the dislocation line and its Burgers vector). This only occurs when ν falls outside the range $[-1, 0.5]$, which is consistent with the statement that sharp corners on equilibrated dislocations are only possible in highly anisotropic crystals. However, the equilibrium loop shapes predicted by isotropic elasticity line tension models using Scattergood and Bacon's effective moduli are likely to match anisotropic elasticity results (DD and line tension) better than those using Voigt or Reuss average moduli, as we will see in the next section.

5. Results

In this section we present the simulation results for the four cases described in table 1. We compare the full anisotropic method implemented using DD, the anisotropic line tension given

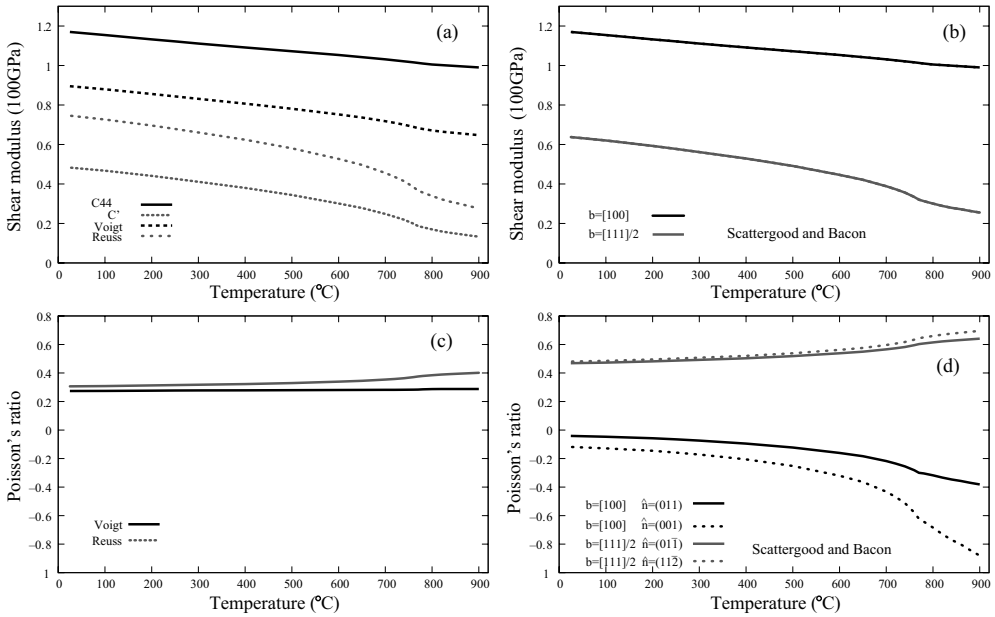

Figure 2. Different average isotropic elastic constants used to compare with anisotropic elastic constants. (*a*), (*c*) The Reuss and the Voigt averages. (*b*), (*d*) The Scattergood and Bacon's averages for different slip systems.

Table 1. Burgers vector $\boldsymbol{b}$, glide plane normal $\hat{\boldsymbol{n}}$ of the bcc lattice.

Case	Burgers vector $\boldsymbol{b}$	Glide plane normal $\hat{\boldsymbol{n}}$
1	[1 0 0]	(0 1 1)
2	[1 0 0]	(0 0 1)
3	$\frac{1}{2}$[1 1 1]	(0 1 $\bar{1}$)
4	$\frac{1}{2}$[1 1 1]	(1 1 $\bar{2}$)

in [13] and the three different isotropic approximations given by the Voigt, the Reuss and the Scattergood and Bacon shear modulus and Poisson's ratio.

In the case of the full anisotropic method, the loops are initialized as circles, and then allowed to relax under the self- and interaction forces on the segments, subject to the constraint that their area remains constant. The area constraint is equivalent to an applied stress that stabilizes the shear loops (see appendix). The core cut-off parameter is equal to the norm of the Burgers vector $\boldsymbol{b}$. In all cases 1–4, a core energy per unit length of $\mu|\boldsymbol{b}|^2/4\pi$ is added to the dislocations to enhance numerical stability in both isotropic and anisotropic elasticity. For isotropic elasticity simulations, the value of μ in the core energy expression equals to either μ_{V}, μ_{R} or μ_{S}, depending on the type of average procedure used. For anisotropic elasticity simulations, the value of μ in the core energy expression is chosen to be μ_{R}. While enhancing the numerical stability, the core energy term is believed to be small enough and to have a negligible effect on the equilibrium shape of the dislocation loops. This has been verified for cases 1 and 2.

Figure 3 shows the equilibrium shapes for shear loops in the four principal slip systems of bcc Fe, calculated using the empirical elastic moduli for 900 °C, and also the Reuss and Voigt averages of those moduli. The most striking features appear in the [1 0 0] systems, where

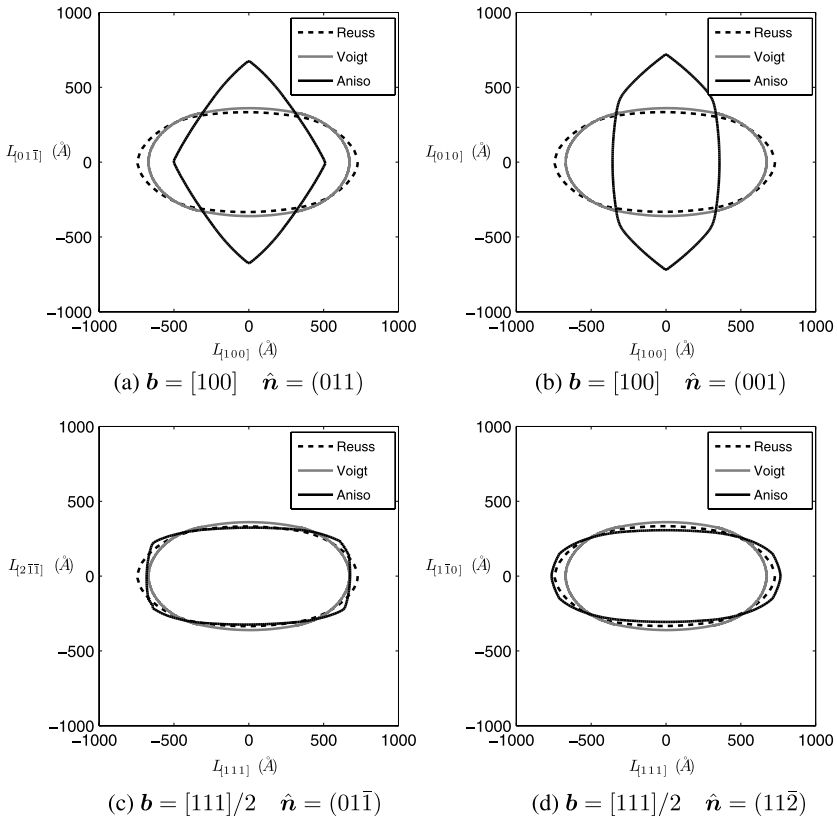

(a) $\boldsymbol{b} = [100] \quad \hat{\boldsymbol{n}} = (011)$ (b) $\boldsymbol{b} = [100] \quad \hat{\boldsymbol{n}} = (001)$

(c) $\boldsymbol{b} = [111]/2 \quad \hat{\boldsymbol{n}} = (01\bar{1})$ (d) $\boldsymbol{b} = [111]/2 \quad \hat{\boldsymbol{n}} = (11\bar{2})$

Figure 3. Equilibrium shapes of dislocation loops relaxed from circular loops of radius 500 Å under the constant area constraint at 900 °C. DD simulation results from isotropic elasticity using Reuss and Voigt averages and from full anisotropic elasticity (Aniso) are superimposed for comparison. Voigt and Reuss approximations do not capture the sharp corners of anisotropic elasticity and the overall shapes are very different.

the departure from the isotropic result is most significant. In both [1 0 0] cases, sharp corners allow the dislocation to completely avoid the screw orientation. This is because the energy of the [1 0 0] screw relative to the [1 0 0] edge increases markedly as C' falls [18]. This cannot be captured by a conventional isotropic formulation for a positive Poisson's ratio, as shown in figure 2, since in this case the screw energy is *always* lower than the edge. This is reflected in the Reuss average results by the alignment of the ellipse's major axis along the screw direction in both [1 0 0] cases. The $\frac{1}{2}$[1 1 1] cases are in much closer agreement. The Reuss average shear modulus is rather lower, better capturing the fall in C', and the $\frac{1}{2}$[1 1 1] cases are less sensitive to the difference between C_{44} and C' than the [1 0 0] cases.

The deformation of Fe at low temperature is widely believed to be governed by the motion of $\frac{1}{2}$[1 1 1] dislocations, though at elevated temperatures this is no longer necessarily the case. The dislocation energetics are very sensitive to the level of anisotropy, and above around 500 °C, various [1 0 0] orientations become energetically favorable, despite having a larger $|\boldsymbol{b}|^2$ than the corresponding $\frac{1}{2}$[1 1 1] cases [5, 6]. This underlines the importance of considering all dislocation species when modeling the deformation of highly anisotropic crystals.

Figure 4 shows the same anisotropic shapes, compared with the shapes predicted by full isotropic elasticity and using the Scattergood and Bacon values of μ and ν. The approximation

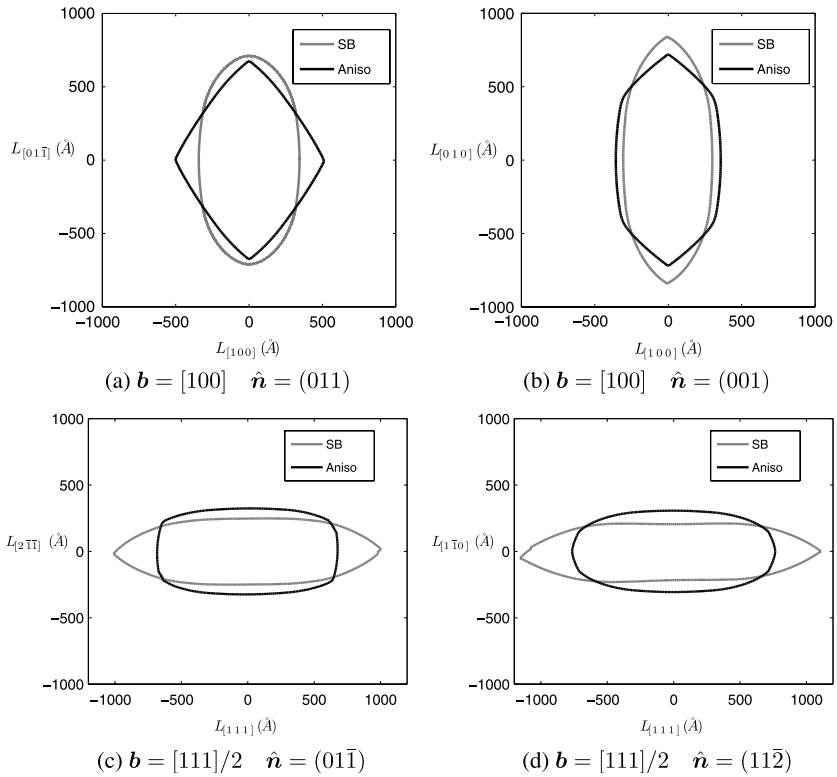

(a) $\boldsymbol{b} = [100] \quad \hat{\boldsymbol{n}} = (011)$ (b) $\boldsymbol{b} = [100] \quad \hat{\boldsymbol{n}} = (001)$

(c) $\boldsymbol{b} = [111]/2 \quad \hat{\boldsymbol{n}} = (01\bar{1})$ (d) $\boldsymbol{b} = [111]/2 \quad \hat{\boldsymbol{n}} = (11\bar{2})$

Figure 4. Equilibrium shape of dislocation loops relaxed from circular loops of radius 500 Å under the constant area constraint at 900 °C. DD simulation results from isotropic elasticity using Scattergood and Bacon (SB) averages and from full anisotropic elasticity (Aniso) are superimposed for comparison.

is much better, even capturing the sharp corner avoiding the [1 0 0] screw in the [1 0 0](0 0 1) case. This is not surprising since the Scattergood and Bacon's averages are slip-system dependent, and hence are not true isotropic moduli. They capture the orientation dependence of the dislocation energies by definition, and hence provide a much closer fit to the full anisotropic results.

Figure 5 shows the effect of the core energy on the equilibrium shape of the dislocation loop, for the example of case 4. Without this core energy term, the elastic instabilities encountered near the [1 $\bar{1}$ 0] orientations lead to the zig–zag behavior of the dislocation loop. The introduction of a core energy acts to smooth out the zig-zags by introducing an additional energy penalty on increasing the dislocation line length. An estimate for this value can be inferred from atomistic simulations [26], but more simulations will be necessary to reliably determine this parameter for the extremely anisotropic crystal considered here. If core energy is not added, the same zig-zag behavior is exhibited in case 3, but not in cases 1 and 2. For consistency, we added the same core energy in all four cases considered in this work.

Figure 6 compares the full anisotropic simulation loop shapes with those derived using the analytical anisotropic line tension model [4, 13]. The two sets of predictions are in good qualitative agreement. For example, the cusps in case 3 are reproduced in both models, in agreement with [10, 11]. However, there are also differences between the DD and line tension model predictions. In case 2, i.e. $\boldsymbol{b} = [1\,0\,0]$ and $\hat{\boldsymbol{n}} = (0\,0\,1)$, the DD prediction at $T = 900\,^{\circ}\mathrm{C}$

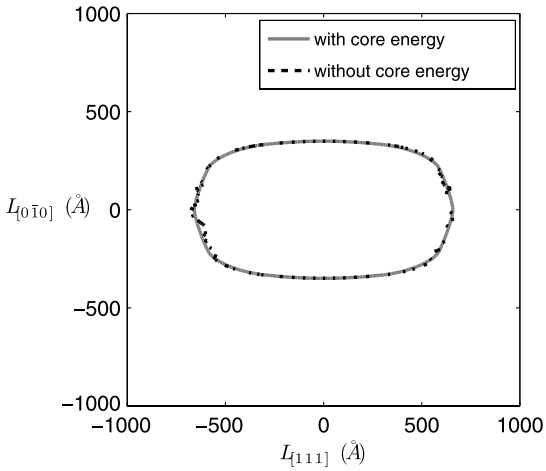

Figure 5. Equilibrium shape of dislocation loops in full anisotropic simulation when the core energy is added (solid line) and when it is not (dots). This corresponds to case 4 in table 1 with $\boldsymbol{b} = [111]/2$ and $\hat{\boldsymbol{n}} = (11\bar{2})$ at 900 °C starting with a circular loop with radius 500 Å under the constant area constraint. Without core energy, the dislocation exhibits instabilities on the left and right sides of the loop.

appears more elongated in the [0 1 0] direction than the line tension model prediction. This is further illustrated by figure 7. In case 3, i.e. $\boldsymbol{b} = [1\,1\,1]/2$ and $\hat{\boldsymbol{n}} = (0\,1\,\bar{1})$, the line tension model predictions appear more elongated in the [1 1 1] direction than the DD predictions. It is of interest to identify the causes for the differences between the DD and line tension model predictions. We have verified that (for case 2) the addition of the core energy in the DD model has a negligible effect on the equilibrium loop shape. It tends to smooth out sharp corners, and may be responsible for the differences in the upper-right and lower-left corners of the loop in case 3 at $T = 900\,^{\circ}\mathrm{C}$.

We believe the differences in the aspect ratio of the equilibrium dislocation loops are caused by the dislocation interaction energies in the full elasticity (DD) model that is not present in the local line tension model. However, the full elasticity model is expected to reduce to the line tension model in the limit of infinitely large dislocation loops. We have verified that this is indeed the case, by repeating the simulation in case 2, starting from a circular dislocation loop with radius 1000 Å, i.e. twice as that used in figure 6. This leads to a better agreement between the DD and line tension model predictions. Therefore, we conclude that the differences observed here are a finite-size effect and that the equilibrium shape of dislocation loops smaller than the sizes considered here is expected to deviate from the line tension model predictions.

The DD method used in `ParaDiS` computes forces. They can numerically be integrated to compute the energy of a dislocation loop as explained in the appendix. The energy comparisons give an indication of how close the different isotropic approximations are to the anisotropic solution and complement the observations made by comparing their shapes.

Figure 8(*a*) plots the loop energies predicted by anisotropic elasticity at different temperatures. As expected, the loop energies decrease with temperature. The energies of loops with $\boldsymbol{b} = [1\,0\,0]$ (cases 1 and 2) are larger than those with $\boldsymbol{b} = \frac{1}{2}[1\,1\,1]$ (cases 3 and 4), for the same loop area. As temperature rises, the differences between the loop energies in cases 1 and 2 and those in cases 3 and 4 decrease, suggesting that dislocations with $\boldsymbol{b} = [1\,0\,0]$ will play a greater role as temperature increases. Figure 8(*b*) shows how the three different isotropic

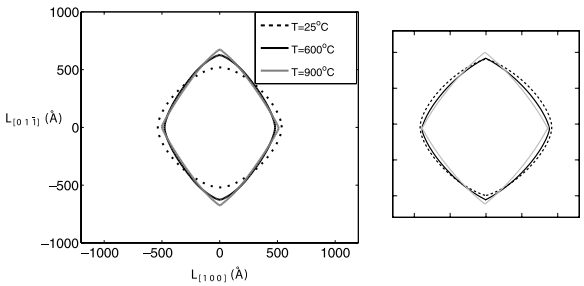

(a) $\boldsymbol{b} = [100]$ $\hat{\boldsymbol{n}} = (011)$

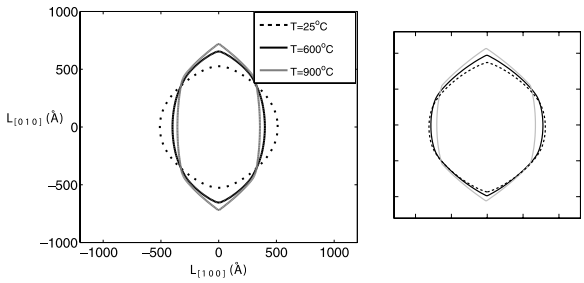

(b) $\boldsymbol{b} = [100]$ $\hat{\boldsymbol{n}} = (001)$

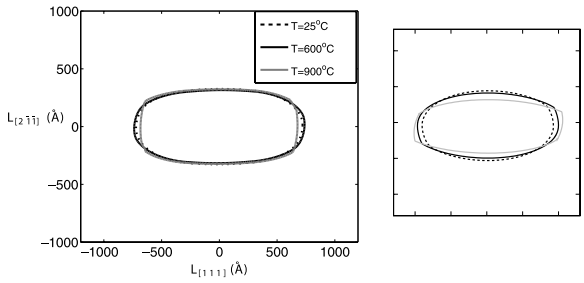

(c) $\boldsymbol{b} = [111]/2$ $\hat{\boldsymbol{n}} = (01\bar{1})$

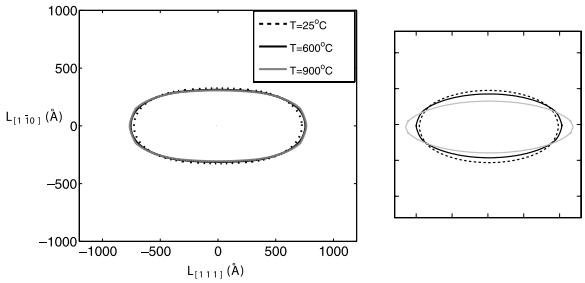

(d) $\boldsymbol{b} = [111]/2$ $\hat{\boldsymbol{n}} = (11\bar{2})$

Figure 6. Equilibrium shapes of dislocation loops under the constant area constraint. Left column: relaxed shapes from circular loops of radius 500 Å using full anisotropic elasticity DD simulations. Right column: predictions from the line tension model.

approximations compare with anisotropic elasticity at $T = 900\,^{\circ}\mathrm{C}$. It shows that the energy values from anisotropic elasticity are always lower than those from the Voigt approximation, and higher than those from the Reuss approximation. Although it gives better predictions for the equilibrium shapes, the Scattergood and Bacon approximations exaggerate the relative

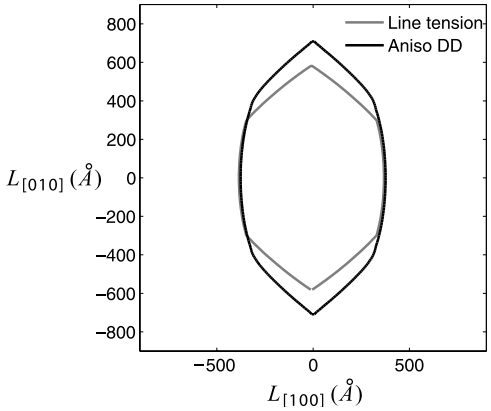

Figure 7. The black line is the relaxed dislocation loop by full anisotropic DD simulation starting from circular loops of radius 500 Å under the constant area constraint. The gray line is the equilibrium shape predicted by the line tension model, uniformly scaled to match the dimension of the DD prediction in the horizontal axis.

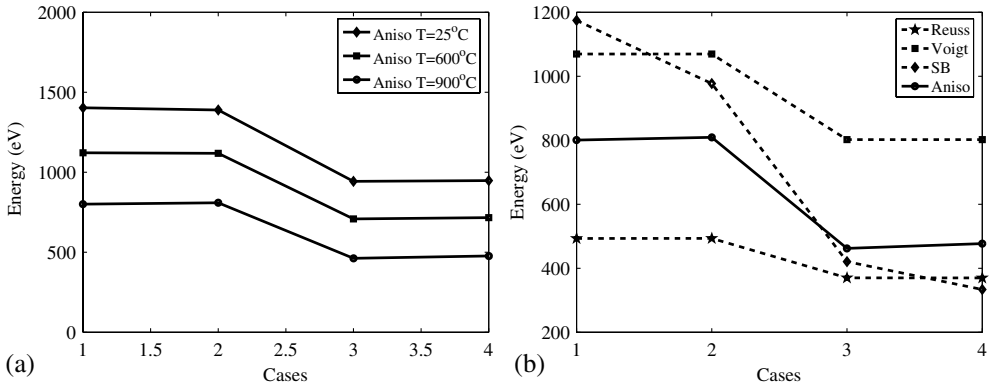

Figure 8. (*a*) Energy of four types of dislocation loops with the same area at three different temperatures predicted by anisotropic elasticity and isotropic elasticity using the Scattergood and Bacon averaged moduli. (*b*) Energy comparisons between anisotropic elasticity and different isotropic approximations: Voigt, Reuss and Scattergood and Bacon's (SB) at $T = 900\,^{\circ}$C. The lines are a guide for the eyes only.

energy difference between loops on different slip systems, most likely because it uses different elastic moduli for different slip systems.

6. Conclusions

Using fully interacting three-dimensional anisotropic elasticity DD simulations, we have shown that the equilibrium configurations of dislocations in highly anisotropic α-Fe exhibit sharp corners, and that no globally averaged effective isotropic moduli can capture them. We have also shown that the sharp corners can in principle be modeled using an isotropic elasticity model, via the Scattergood and Bacon approximation, provided that the stability constraint $\nu \in [-1, 0.5]$ is violated. Although the Scattergood and Bacon model may produce results in reasonable agreement with the full anisotropic calculations for a dislocation loop in one plane, the full anisotropic elasticity approach is necessary when modeling dislocations occupying

multiple planes in three dimensions, since Scattergood and Bacon's method does not provide a unique pair of elastic constants μ and ν for different slip systems.

The sharp corners are a direct result of the emerging thermodynamical instability of certain dislocation orientations as the crystal anisotropy is increased. The structures we predict are consistent with those observed in the microscope [10, 11] (see also [27]), and with the analytical modeling approach described earlier. These insights will aid future attempts to model yield and plastic flow in the highly anisotropic limit.

Acknowledgments

The authors thank Professor D M Barnett for countless stimulating discussions and helpful suggestions, and Mr J Yin for helping us implement the algorithms described in [16]. S Aubry is supported by the Army High Performance Computing Research Center at Stanford. S Fitzgerald and S Dudarev are supported by the European Communities under the contract of Association between EURATOM and CCFE, was carried out within the framework of the European Fusion Development Agreement. The views and opinions expressed herein do not necessarily reflect those of the European Commission. This work was also part-funded by the RCUK Energy Programme under grant EP/G003955.

Appendix. Details of the dislocation dynamics method

The DD method used in this paper is described in [21]. This method was extended to anisotropic elasticity which is described in [16, 18]. The DD method was modified further to obtain the results shown in this paper. We present the modifications in this appendix.

A.1. Area constraint

The DD method is used to determine the relaxed shape of a dislocation loop and compute its energy. When a dislocation loop is relaxed using DD, its area either shrinks or expands depending on the applied stress. This is prevented by the use of a Lagrange multiplier which enforces the constraint that the area of the loop remains constant.

The energy minimization is under the constraint that the area $\mathcal{A}$ is always equal to the initial area, i.e.

$$\min_{\mathcal{A}(\{\boldsymbol{r}_i\})=A_0} E(\{\boldsymbol{r}_i\})$$

where $\boldsymbol{r}_i$ are position of the nodes sampling the dislocation loops. To solve this problem, we introduce a Lagrange multiplier λ, and study the Lagrange function defined by

$$\Lambda(\{\boldsymbol{r}_i\}, \lambda) = E(\{\boldsymbol{r}_i\}) - \lambda(\mathcal{A}(\{\boldsymbol{r}_i\}) - A_0)$$

and then find solutions to the equation

$$\nabla_{r_i,\lambda}\Lambda(\{\boldsymbol{r}_i\}, \lambda) = 0.$$

This means

$$\nabla_{\lambda}\Lambda(\{\boldsymbol{r}_i\}, \lambda) = \mathcal{A}(\{\boldsymbol{r}_i\}) - A_0 = 0$$

and

$$\nabla_{r_i}\Lambda(\{\boldsymbol{r}_i\}, \lambda) = -\boldsymbol{F}_i + \lambda\, \boldsymbol{g}_i = 0, \tag{A.1}$$

where $\boldsymbol{F}_i \equiv -\nabla_{r_i} E(\{\boldsymbol{r}_i\})$ is the force on node i, and $\boldsymbol{g}_i \equiv -\nabla_{r_i}\mathcal{A}(\{\boldsymbol{r}_i\})$.

One way to solve this problem iteratively is to update dislocation nodal positions by

$$\boldsymbol{r}_i{}^{n+1} = \boldsymbol{r}_i{}^n - \tilde{\boldsymbol{F}}_i^n \cdot \Delta t,$$

where

$$\tilde{\boldsymbol{F}}_i^n = \boldsymbol{F}_i{}^n - \frac{\sum_j \boldsymbol{F}_j{}^n \cdot \boldsymbol{g}_j^n}{\sum_j |\boldsymbol{g}_j^n|^2}\, \boldsymbol{g}_i^n. \tag{A.2}$$

with $\boldsymbol{F}_i{}^n = -\nabla_{r_i} E(\{\boldsymbol{r}_i^n\})$ and $\boldsymbol{g}_i^n = -\nabla_{r_i} A(\{\boldsymbol{r}_i^n\})$. In DD simulations, this means using a mobility law $\boldsymbol{v}_i = \boldsymbol{F}_i$ and modifying the nodal force according to equation (A.2). When the relaxation converges, $\boldsymbol{F}_i{}^n$ will be parallel to $\boldsymbol{g}_i^n$, as required by equation (A.1), and $\tilde{\boldsymbol{F}}_i^n = 0$.

Since we are searching for the equilibrium dislocation shape at which the force on the dislocation vanishes, the result should be independent of the magnitude of dislocation mobility. The fact that edge dislocations move faster than screw dislocations in bcc Fe can affect the shape of an expanding dislocation loop, but has no effect on the equilibrium shape of a dislocation loop.

A.2. Energy calculations

`ParaDiS` computes the driving force $\boldsymbol{F}_i$ at node i as described in detail in [16, 21]. In the bulk, this force is the sum of three forces described in section 3. The total energy of the dislocation loop can be computed by integrating the force on all the nodes as the loop continuously shrinks to zero radius.

Let $\{\boldsymbol{r}_i\}$, $i = 0, \ldots, N$, be the positions of nodes in the loop. Now consider a series of loops defined by nodes at positions $\{\alpha \boldsymbol{r}_i\}$. As α goes from 0 to 1, the loop continuously scales from radius zero to the current size.

$$\begin{aligned} E_{\text{tot}} = E(\{\boldsymbol{r}_i\}) &= \int_0^1 \frac{\mathrm{d}E(\{\alpha \boldsymbol{r}_i\})}{\mathrm{d}\alpha}\, \mathrm{d}\alpha \\ &= -\sum_{j=0}^{N} \int_0^1 \boldsymbol{F}_j(\{\alpha \boldsymbol{r}_i\}) \cdot \boldsymbol{r}_j\, \mathrm{d}\alpha, \end{aligned}$$

where $\boldsymbol{F}_j$ is the force on node j for loop $\{\alpha \boldsymbol{r}_i\}$.

The integral over α is evaluated by quadrature over a uniform grid with grid size $\Delta\alpha = \frac{1}{500}$.

References

[1] Dever D J 1972 Temperature-dependence of the elastic constants in α-iron single crystals: relationship to spin order and diffusion anomalies *J. Appl. Phys.* **43** 3293

[2] Zinkle S J and Ghoniem N M 2000 Operating temperature windows for fusion reactor structural materials *Fusion Eng. Des.* **51** 55–71

[3] Fitzgerald S P and Dudarev S L 2008 Dislocation pile-ups in Fe at high temperature *Proc. R. Soc. Lond.* A **464** 2549–59

[4] Fitzgerald S P 2010 Frank–Read sources and the yield of anisotropic cubic crystals *Phil. Mag. Lett.* **90** 209–18

[5] Dudarev S L, Bullough R and Derlet P M 2008 Effect of the α–γ phase transition on the stability of dislocation loops in bcc iron *Phys. Rev. Lett.* **100** 135503

[6] Fitzgerald S P and Yao Z 2009 Shape of prismatic dislocation loops in anisotropic α-Fe *Phil. Mag. Lett.* **89** 581–8

[7] Head A K 1967 Unstable dislocations in anisotropic crystals *Phys. Status Solidi* **19** 185–92

[8] Head A K, Loretto M H and Humble P 1967 The influence of large elastic anisotropy on the determination of burgers vectors of dislocations in beta brass by electron microscopy *Phys. Status Solidi* **20** 505–19

[9] Head A K, Loretto M H and Humble P 1967 The identification of Burgers vectors and unstable directions of dislocations in beta brass *Phys. Status Solidi* **20** 521–36

[10] Caillard D 2009 TEM *in situ* straining experiments in Fe at low temperature *Phil. Mag. Lett.* **89** 517–26

[11] Caillard D 2010 Kinetics of dislocations in pure Fe: I. *In situ* straining experiments at room temperature *Acta Mater.* **58** 3493–3503
[12] Douin J, Veyssiere P and Beauchamp P 1986 Dislocation line stability in Ni_3Al *Phil. Mag.* A **54** 375–93
[13] Bacon D J, Barnett D M and Scattergood R O 1980 Anisotropic continuum theory of lattice defects *Prog. Mater. Sci.* **23** 51–262
[14] Han H, Ghoniem N M and Wang Z 2003 Parametric dislocation dynamics of anisotropic crystals *Phil. Mag.* **83** 3705–21
[15] Rhee M, Stolken J S, Bulatov V V, de la Rubia T D, Zbib H M and Hirth J P 2001 Dislocation stress fields for dynamic codes using anisotropic elasticity: methodology and analysis *Mater. Sci. Eng.* A **309** 288–93
[16] Yin J, Barnett D M and Cai W 2010 Efficient computation of forces on dislocation segments in anisotropic elasticity *Modelling Simul. Mater. Sci. Eng.* **18** 045013
[17] Cai W, Arsenlis A, Weinberger C R and Bulatov V V 2006 A non-singular continuum theory of dislocations *J. Mech. Phys. Solids* **54** 561–87
[18] Fitzgerald S P and Aubry S 2010 Self force on dislocation segments in anisotropic crystals *J. Phys.: Conden. Matter* **22** 295403
[19] Scattergood R O and Bacon D J 1975 The Orowan mechanism in anisotropic crystals *Phil. Mag.* **31** 179–98
[20] deWit G and Koehler J S 1959 Interaction of dislocations with an applied stress in anisotropic crystals *Phys. Rev.* **116** 1113–20
[21] Arsenlis A, Cai W, Tang M, Rhee M, Oppelstrup T, Hommes G, Pierce T G and Bulatov V V 2007 Enabling strain hardening simulations with dislocation dynamics *Modelling Simul. Mater. Sci. Eng.* **15** 553–95
[22] Mura T 1963 Continuous distribution of moving dislocations *Phil. Mag.* **8** 843–57
[23] Voigt W 1928 *Lehrbuch der Kristallphysik* (Leipzig: Teubner) p 962
[24] Reuss A 1929 Berechnung der fliessgrenze von mischkristallen auf grund der plastitatsbedingung für einkristalle *Z. Angew. Math. Mech.* **9** 49–58
[25] Ting T C T and Barnett D M 2005 Negative Poisson's ratios in anisotropic linear elastic media *J. Appl. Mech.* **72** 929
[26] Bulatov V V and Cai W 2006 *Computer Simulations of Dislocations* (Oxford: Oxford University Press)
[27] Boutard J-L, Dudarev S and Rieth M 2011 *J. Nucl. Mater.* at press (doi:10.1016/j.jnucmat.2010.12.293)